

Article

Virtual Synchronous Control Based on Control Winding Orientation for Brushless Doubly Fed Induction Generator (BDFIG) Wind Turbines Under Symmetrical Grid Faults

Min Lu ^{1,2}, Yu Chen ^{1,*}, Debin Zhang ¹, Jingyuan Su ¹ and Yong Kang ¹

¹ State Key Laboratory of Advanced Electromagnetic Engineering and Technology (AEET), Huazhong University of Science and Technology (HUST), Wuhan 430074, China; lm_hust@hust.edu.cn (M.L.); zhangdebin@hust.edu.cn (D.Z.); sujingyuan@hust.edu.cn (J.S.); ykang@mail.hust.edu.cn (Y.K.)

² College of Mechanic & Electrical Engineering, Shihezi University, Shihezi 832000, China

* Correspondence: ayu03@hust.edu.cn

Received: 2 December 2018; Accepted: 17 January 2019; Published: 20 January 2019



Abstract: The Brushless Doubly Fed Induction Generator (BDFIG) has huge potential for wind power systems due to its high reliability and low maintenance cost. To add inertia for system stability enhancement, as well as to maintain the uninterrupted operation during symmetrical grid faults, this study proposes a Virtual Synchronous Control (VSC) with a transient current compensation strategy for BDFIG. The proposed VSC is realized by regulating the virtual inner electrical potential and angular velocity of BDFIG under Control Winding (CW) current oriented vector control, and compensating for the transient CW current to weaken the transient inner electrical potential under symmetrical grid faults. Modeling and analysis of such a VSC strategy are presented in this paper, and a simulation is also made to compare the performances of existing and proposed VSC strategies. It is shown that the merits of the proposed VSC can enhance the fault ride through the ability of the BDFIG system and support the recovery of grid voltage.

Keywords: Brushless Doubly Fed Induction Generator (BDFIG); power electronic interface; Virtual Synchronous Control (VSC); transient characteristics; CW current compensation

1. Introduction

Wind is a kind of economical and clean renewable resource, and with the developing maturity of technology, wind energy has become one of the most popular renewable energies for electrical power generation. However, wind power inherits intermittent and random characteristics, which is very different from conventional power from the Synchronous Generator (SG). When large-scale wind power is connected to the power grid, the stability of the whole power system will be inevitably impacted. This is because wind turbines connect to the power grid via power electronics interfaces, and the controllers of traditional power electronics interfaces aim to make the active power and reactive power track to the references with a fast response, without considering the voltage/frequency states of the power grid. Therefore, the high penetration level of wind turbines and power electronics interfaces will decrease the total system inertia and lower the voltage/frequency stabilization compared to conventional synchronous generating units. The large voltage/frequency deviation might result in separation of the power system [1–4].

The Brushless Doubly Fed Induction Generator (BDFIG) is a cost-efficient component employed to turn the mechanical power of a wind turbine to electric power. As shown in Figure 1, BDFIG adopts a dual-stator structure, namely Power-Winding (PW) and Control-Winding (CW), to eliminate

brushes and slip rings. Such a brushless structure not only improves the reliability and reduces the maintenance cost, but also preserves the Variable Speed Constant Frequency (VSCF) characteristic, which is similar to the conventional Doubly-Fed Induction Generator (DFIG). The structure diagram of a BDFIG system suitable for a wind power application is also illustrated in Figure 1. A Back-to-Back (B2B) converter is utilized as a bridge between the CW and the power grid, and its capacity can be much smaller than that of BDFIG since it only needs to handle the slip power. The grid-side of the B2B converter is utilized to maintain a stable dc-link voltage, while the CW-side of the B2B converter is utilized to control the active power and reactive power injected into the grid. The vector control is mostly used for BDFIG control [5–8].

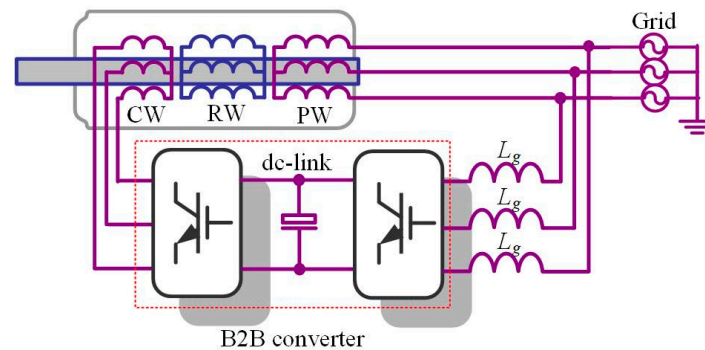


Figure 1. The overview of the BDFIG wind power system. CW: Control-Winding; RW: Rotor-Winding; PW: Power-Winding.

When introducing BDFIG into a wind power application, a mandated requirement is that the BDFIG should realize low-voltage ride through LVRT. Some LVRT studies for the BDFIG system have been presented. Reference [9] showed the dynamic analysis of the BDFIG during symmetrical voltage dips, and proposed a control strategy applied to the CW-side converter to inject reactive power to the grid when a grid fault occurred. References [10,11] compared the LVRT performances of DFIG and BDFIG, and proved that BDFIG had some advantages over DFIG in LVRT performances, because the magnitude of the CW transient current in BDFIG was lower than that of the rotor current in DFIG during grid faults. Reference [12] discussed the rotor winding (RW) issues of BDFIG and studied the dynamic characteristics when the grid voltage dropped.

The recent controls for the BDFIG system use phase-locked loops (PLLs) to synchronize the vector control system with the grid voltage, and such controls have no contribution to the system stability. Recently, many control methods, such as virtual inertia control [13,14], droop control [15], pitch angle control [16], coordinated control [17], and the virtual synchronous generator [18], have been proposed for DFIG or grid-tied converters. Among them, the virtual synchronous generator uses extra short-term energy storage units plus Virtual Synchronous Control (VSC) to simulate the virtual rotor inertia [19,20]. VSC makes the DFIG or grid-tied converter respond to the frequency change of grid, alleviating the system stability problem, which is deteriorated by the Phase-Locked Loop (PLL) [21]. However, VSC for the BDFIG system has not yet been widely discussed.

This paper introduces VSC into the BDFIG system, so that the BDFIG can not only provide inertia to the grid, but also improve the transient characteristics during LVRT. The proposed VSC is realized by regulating the virtual inner electrical potential and angular velocity of BDFIG under Control Winding (CW) current oriented vector control, and compensating for the transient CW current to weaken the transient inner electrical potential under symmetrical grid faults. Such a control makes the behavior of BDFIG similar to SG; when a grid fault occurs, such a control can reduce the CW overcurrent and maintain an uninterrupted operation; and when the grid fault is cleared, such a control can inject reactive power into the grid to assist with grid recovery. Modeling and analysis of the proposed control are presented in Sections 2 and 3, respectively; the control strategy is given in Section 4; a simulation is

also made in Section 5 to compare the performances of existing and proposed VSC strategies; and the conclusion is given in Section 6.

2. Virtual Synchronization Mechanism for BDFIG

2.1. The Characteristics of SG

To realize the proposed control, the dynamics of SG should be surveyed first. Here, the classical second-order SG model [22] is used:

$$\begin{cases} U_g \angle 0 = -R_\sigma I_g \angle \sigma - L_\sigma \frac{d}{dt} I_g \angle \sigma + E_0 \angle \delta \\ E_0 \angle \delta = M_f I_f \omega_0 \sin \theta \\ T_m - T_e - D(\omega_0 - \omega_{ref}) = J \frac{d\omega_0}{dt} \\ \theta = \int \omega_0 dt \end{cases} \quad (1)$$

where $U_g \angle 0$ is the generator port voltage vector, and also the grid voltage when SG is connected to the grid. It is treated as the phase reference; $I_g \angle \sigma$ is the current injected into the grid, of which σ is the power factor angle; $E_0 \angle \delta$ is the inner electrical potential, of which δ is the power angle; M_f is the coefficient of mutual induction; I_f is the exciting current; θ is the rotor angle and $\sin \theta = [\sin \theta \sin(\theta - 120^\circ) \sin(\theta + 120^\circ)]$; T_m is the mechanical torque; T_e is the electromagnetic torque; J is the moment of inertia; D is the damping coefficient; ω_0 is the electrical angular velocity of the inner electrical potential; and ω_{ref} is the rated electrical angular velocity.

The characteristics of SG can be well-described by the above mathematical model: when the power is unbalanced, the angular velocity ω_0 and the inner electrical potential $E_0 \angle \delta$ will change. Due to the existence of inertia J , SG has the inertia during the power and frequency dynamical process, and the damping coefficient D makes SG have the capability of damping oscillation.

2.2. Equivalent Model of BDFIG

BDFIG adopts the non-coupled dual-stator winding structure with different numbers of poles. Denoting the pole-pair number of PW as p_p and the pole-pair number of CW as p_c , the following relation can be given:

$$\omega_r = \frac{\omega_p - \omega_c}{p_p + p_c} \quad (2)$$

where ω_p , ω_c , and ω_r are the angular velocities of PW, CW, and RW, respectively.

When the PW is connected to the grid, the PW frequency ω_p is the grid frequency. According to Equation (2), ω_c can be controlled by the CW-side of the B2B converter to maintain VSCF, even when ω_r is varied. The BDFIG can work in sub-synchronous, synchronous, and super-synchronous modes, depending on ω_r ; and the slip power flowing through the B2B converter can be dual-direction, depending on the modes of BDFIG.

The mathematical model of BDFIG is shown in Equation (3). In order to convert the voltage equation of the PW into a form similar to SG, the PW, CW, and RW adopt the generator conventions [23].

$$\begin{cases} \vec{u}_p = -R_p \vec{i}_p + \frac{d\vec{\varphi}_p}{dt} + j\omega_{pc} \vec{\varphi}_p \\ \vec{\varphi}_p = -L_p \vec{i}_p + L_{s1r} \vec{i}_r \\ \vec{u}_c = -R_c \vec{i}_c + \frac{d\vec{\varphi}_c}{dt} + j\omega_c \vec{\varphi}_c \\ \vec{\varphi}_c = -L_c \vec{i}_c + L_{s2r} \vec{i}_r \\ \vec{u}_r = R_r \vec{i}_r + \frac{d\vec{\varphi}_r}{dt} + j\omega_{cr} \vec{\varphi}_r \\ \vec{\varphi}_r = L_r \vec{i}_r - L_{s1r} \vec{i}_p - L_{s2r} \vec{i}_c \end{cases} \quad (3)$$

where \vec{x} denotes a vector; $\omega_{pc} = \omega_c + (p_p + p_c)\omega_r$; and $\omega_{cr} = \omega_c - p_c\omega_r$.

To facilitate the later SVG control, the model of BDFIG in Equation (3) is turned into the following equivalent form:

$$\begin{cases} U_p \angle \theta_{pc} = -R_p I_p \angle (\theta_{pc} + \sigma) - (L_p - L_{s1r} k_1) \frac{dI_p \angle (\theta_{pc} + \sigma)}{dt} + E_0 \angle (\theta_{pc} + \delta) \\ E_0 \angle (\theta_{pc} + \delta) = k_2 L_{s1r} (s + j\omega_p) I_c \angle 0 + j\omega_p (L_{s1r} k_1 - L_p) I_p \angle (\theta_{pc} + \sigma) \end{cases} \quad (4)$$

where $U_p \angle \theta_{pc}$ is the vector of PW voltage; θ_{pc} is the transformation angle between PW voltage and CW current; $k_1 = L_{s1r} / L_r$, $K_2 = L_{s2r} / L_r$; and $I_c \angle 0$ is taken as the angular reference since the d-q synchronous coordinate is aligned with CW current in our design.

Equations in (4) are analogous to the first and second equations in Equation (1), as shown in Figure 2. The basic idea of VSC for BDFIG can thus be obtained:

- In an SG, the magnitude of inner electrical potential E_0 can be regulated by I_f , and analogously, the virtual inner electrical potential E_0 in a BDFIG can be regulated by CW current I_c when the BDFIG parameters and rotor speed are known (the PW current I_p is also regarded as a known quantity since it can be measured directly);
- In an SG, the angular velocity of the inner electrical potential ω_0 is varied during regulation, and analogously, it can be simulated by varying the angular velocity of CW current I_c (in the CW current oriented case, it is equivalent to varying the angular velocity of the d-q synchronous coordinate).

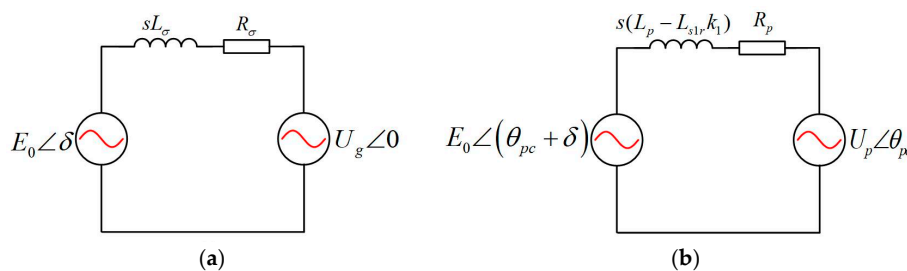


Figure 2. Comparison of the equivalent circuits of (a) Synchronous Generator (SG) and (b) Brushless Doubly Fed Induction Generator (BDFIG).

Before and after such a VSC, the transition of the operation point of BDFIG can also be explained from the SG point of view, as given in Figure 3. By varying I_c^* to a new stable value and varying ω_0^* during transient regulation, both the virtual electrical potential E_0 and the power angle δ are changed. Correspondingly, the PW current I_p also changes its position, and thus, the active power and reactive power are changed.

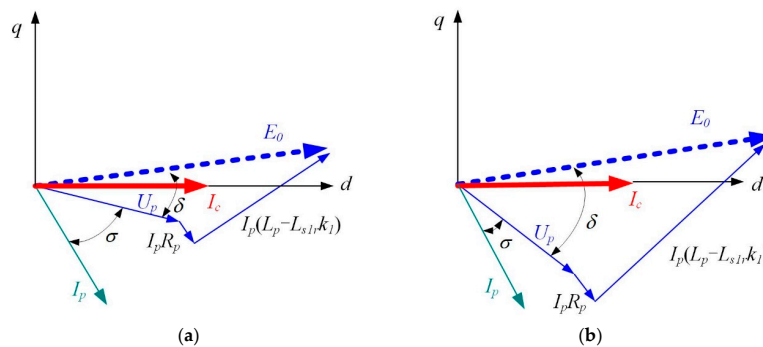


Figure 3. The vector diagrams before and after operation point changes. (a) Before the adjustment; (b) After the adjustment.

3. Transient Characteristics of BDFIG Based on VSC in Symmetrical Grid Faults

Dynamic behavior described by Equation (1) is relatively slow (the regulation usually prolongs tens of fundamental periods or even longer), and therefore, the applicability of the VSC strategy in the case of grid faults needs to be considered. Transient characteristics during a symmetrical grid fault are discussed in this section.

3.1. Model of BDFIG under Symmetrical Grid Faults

The CW voltage of BDFIG can be expressed by the PW flux:

$$\vec{u}_c = \underbrace{L_{k1} \left(\frac{d}{dt} - j\omega_c \right) \vec{\varphi}_p}_{\vec{e}_c} + \underbrace{\left[R_c + L_{k2} \left(\frac{d}{dt} - j\omega_c \right) \right] \vec{i}_c}_{\vec{u}_{c\sigma}} \tag{5}$$

where $L_{k1} = \frac{M_{pr}M_{cr}}{M_{pr}^2 - L_pL_r}$, $L_{k2} = \frac{M_{pr}^2L_c + M_{cr}^2L_p - L_pL_cL_r}{M_{pr}^2 - L_pL_r}$.

Since the d-q synchronous coordinate is aligned with CW-current, the term $j\omega_c \vec{i}_c$ is zero. Equation (5) can be simplified as follows:

$$\vec{u}_c = \underbrace{L_{k1} \left(\frac{d}{dt} - j\omega_c \right) \vec{\varphi}_p}_{\vec{e}_c} + \underbrace{\left(R_c + L_{k2} \frac{d}{dt} \right) \vec{i}_c}_{\vec{u}_{c\sigma}} \tag{6}$$

Equation (6) can be illustrated as Figure 4. It can be divided into two parts. The first part \vec{e}_c is the back electromotive force induced by the PW flux; the second part $\vec{u}_{c\sigma}$ is the voltage drop on the leakage impedance of the CW circuit.

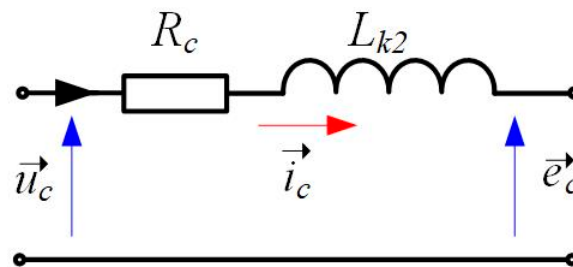


Figure 4. Control Winding (CW) equivalent circuit diagram.

If the terminal voltage amplitude is U_p and the voltage sag is α at $t = 0$, the PW flux can be obtained as follows:

$$\vec{\varphi}_p = \underbrace{\frac{\alpha U_p}{\omega_{pc}} e^{j\theta_{pc0}}}_{\vec{\varphi}_{pw}} + \underbrace{\frac{(1 - \alpha) U_p}{\omega_{pc}} e^{-\frac{t}{\tau_p}} e^{j(\omega_{pc}t + \theta_{pc0})}}_{\vec{\varphi}_{pz}} \tag{7}$$

where θ_{pc0} is the initial transformation angel at the $t = 0$ moment.

Equation (7) can also be divided into two parts. The first term $\vec{\varphi}_{pw}$ is the steady-state component of the PW flux, which is induced by the PW voltage after faults. The second term $\vec{\varphi}_{pz}$ is the transient component of the PW flux, which maintains the PW flux so that it does not mutate at the moment of voltage sag, and recedes to zero with time constant τ_p .

3.2. Compensation Method under CW Current Oriented Coordinate

According to Equation (7), the transient component $\vec{\varphi}_{pz}$ in the CW current oriented coordinate is a sinusoidal waveform with a damped magnitude. We only focus on the non-sinusoidal part:

$$\vec{\varphi}_{pz} = \frac{(1 - \alpha)U_p}{\omega_{pc}} e^{-\frac{t}{\tau_p}} e^{j\theta_{pc}} \quad (8)$$

According to Equation (6), $\vec{\varphi}_{pz}$ will induce a back electromotive force component, which can be expressed as:

$$\vec{e}_{cz} = L_{k1} \left(\frac{d}{dt} - j\omega_c \right) \vec{\varphi}_{pz} = -L_{k1} \left(\frac{1}{\tau_p} + j\omega_c \right) \vec{\varphi}_{pz} \quad (9)$$

Since $1/\tau_p \ll \omega_c$, the $1/\tau_p$ -term can be ignored and (9) can be simplified as:

$$\vec{e}_{cz} \approx -jL_{k1}\omega_c \vec{\varphi}_{pz} \quad (10)$$

According to the CW equivalent circuit in Figure 4, we can compensate for a CW current component i_{cz}^* to cancel \vec{e}_{cz} , which can be obtained as:

$$i_{cz}^* = \frac{jL_{k1}\omega_c \vec{\varphi}_{pz}}{\sqrt{R_c^2 + (\omega_c L_{k2})^2}} \quad (11)$$

$\vec{\varphi}_{pz}$ in Equation (11) can be obtained from the following equation [24]:

$$\vec{\varphi}_{pz} = \vec{\varphi}_p - \vec{\varphi}_{pw} \quad (12)$$

where $\vec{\varphi}_p = L_p \vec{i}_p + L_{pr}(k_1 \vec{i}_p + k_2 \vec{i}_c)$ and $\vec{\varphi}_{pw} = -j\vec{v}_p/\omega_p$.

Since the control system has been aligned with the CW current, i_{cq} is always zero and i_{cd}^* should be applied on the d-axis. It is worth mentioning that we only cancel the non-sinusoidal component of the transient PW flux. Nevertheless, such a compensation can efficiently damp the peak of the transient CW current, especially at the first oscillation period.

4. Configuration of the BDFIG System with the Proposed Control

According to the analysis in Sections 2 and 3, the overall control system is designed, as shown in Figure 5. The design considerations are as follows:

1. The CW current is sampled and transformed as i_{cd} and i_{cq} based on the transform angle θ_c^* . With PI controllers, i_{cd} tracks its reference i_{cd}^* , and i_{cq} tracks to zero. In this way, CW current is always aligned with the d-axis of the synchronous coordinate, realizing CW current orientation. With such an orientation, current limiting can also be easily implemented by setting an upper limit of i_{cd}^* . The outputs of the two PI controllers are u_{cd}^* and u_{cq}^* , and they are transformed back to the abc coordinate based on the transform angle θ_c^* , and utilized to modulate the CW-side of the B2B converter;
2. The active power P and reactive power Q are fed back and compared with the references P^* and Q^* . The errors are sent to the active power and reactive power controllers [25], as the red region shown in Figure 5. It is worth mentioning that such controllers are designed based on the SG in Equation (1), and thus, their outputs, i.e., the magnitude of inner electrical potential E_0^* and its angular velocity ω_0^* , can fully consider the behavior of SG;
3. To realize VSC, the magnitude of the virtual inner electrical potential of BDFIG should track to E_0^* , and its angular velocity should be ω_0^* . Therefore, ω_0^* is integral as θ_p , and then, according to (2), the corresponding angular velocity required by the d-q synchronous coordinate is obtained as θ_c^* .

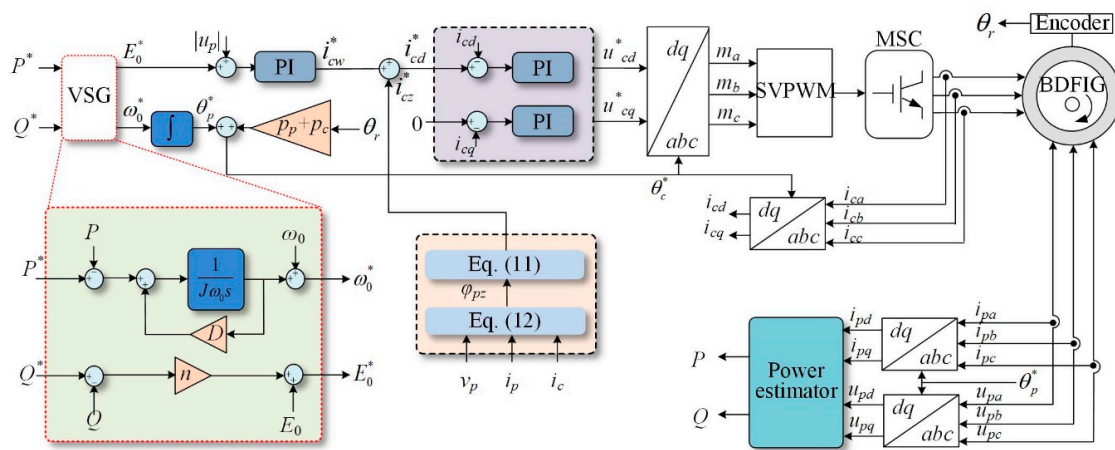


Figure 5. The proposed control block diagram.

Additionally, according to the first equation in (4), E_0 can be obtained as:

$$E_0 = \left| U_p \angle \theta_{pc} + R_p i_p \angle (\theta_{pc} + \sigma) + (L_p - L_{s1r} k_1) \frac{di_p \angle (\theta_{pc} + \sigma)}{dt} \right| \tag{13}$$

To simplify the implementation, the second and third terms in (13) can be ignored since they are small enough compared with the first term, and therefore:

$$E_0 \approx |U_p| \tag{14}$$

As shown in Figure 5, $|U_p|$ is compared with E_0^* , and the error is sent to a PI regulator to generate the steady-state CW current reference i_{cw}^* , and finally E_0 tracks to E_0^* ;

- In order to improve the operation characteristics of BDFIG in the case of symmetrical grid faults, Equations (11) and (12) are utilized to calculate the compensation term i_{cz}^* , and the total reference current $i_{cd}^* = i_{cw}^* + i_{cz}^*$ is finally obtained for the inner CW current controller.

5. The Example Analysis

5.1. BDFIG System Configuration

In order to verify the effectiveness of the VSC strategy with transient current compensation, this paper uses Simulink to build the BDFIG system model. The BDFIG parameters are shown in Table 1.

Table 1. The specifications of the BDFIG prototype.

Parameter	Value	Parameter	Value
PW pole-pair number	2	R_r	0.174 Ω
CW pole-pair number	4	L_{s1}	0.05733 H
Rotor speed range	350–650 r/min	L_{s2}	0.051 H
Power rating	32 kW	L_r	0.09467 H
PW-rated voltage	400 V	L_{s1r}	0.049 H
R_{s1}	0.07726 Ω	L_{s2r}	0.04867 H
R_{s2}	0.10234 Ω		

The test system is illustrated in Figure 6. When the voltage sag occurs in the power grid, the active power cannot be outputted normally. Therefore, the mechanical power and electric power are instantly unbalanced, the rotor speed might be varied, the dc-link voltage of B2B might be unstable, and the

grid-side of the B2B converter might be shutdown. Therefore, several strategies have been considered: (1) Emergency rotor control [24] is adopted for the BDFIG to reduce the active power command value (i.e., to reduce the mechanical torque of the wind turbine); (2) according to [18], some extra short-term energy storage units are added to the dc-link of the B2B converter; and (3) the grid-side of the B2B converter inherits with a current limitation function, so as to limit the maximal current when the grid voltage is faulty. With these implementations, the BDFIG system can continue working during a grid fault, and will finally reach new power balancing.

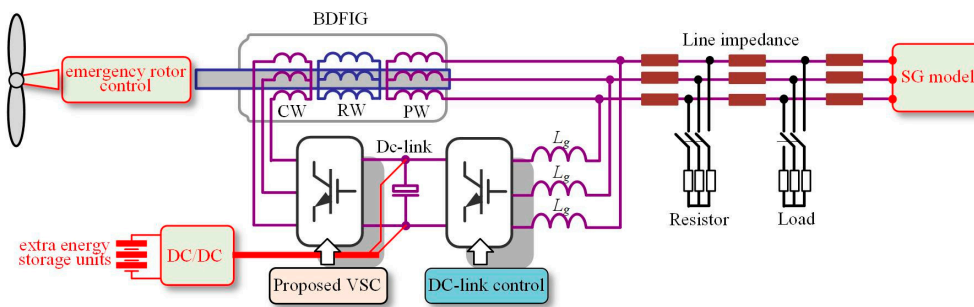


Figure 6. The system model of BDFIG.

The grid-voltage-sag depth directly affects the amplitude of the back electromotive force and CW over the current of BDFIG, and therefore, the simulation will give the waveforms in the cases of a minor fault (30% drop) and deep fault (70% drop).

5.2. Simulation Results

Before the symmetrical fault of the power grid occurs, the PW voltage of BDFIG is in its rated value, the speed is 0.8 pu, and the active power output of PW is 1.0 pu. During simulation, the grid voltage drops to 0.7 pu. The key waveforms of BDFIG are shown in Figure 7, and the active and reactive power of the BDFIG are shown in Figure 8.

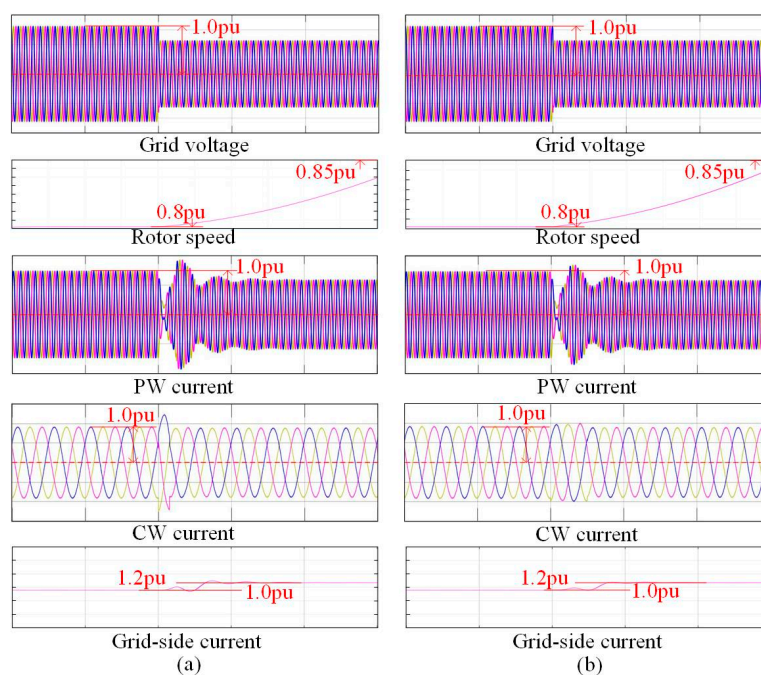


Figure 7. Comparisons of waveforms when the grid has a 30% voltage drop with (a) existing VSC and (b) the proposed VSC ($t: 0.2 \text{ s/div}$).

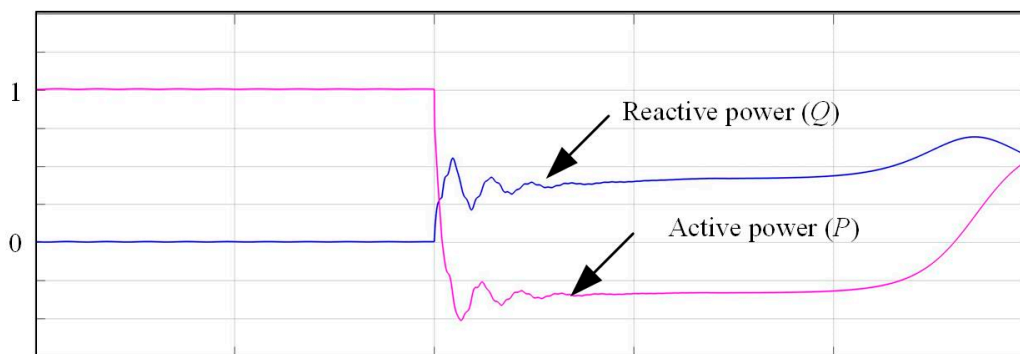


Figure 8. Waveforms of active and reactive power with 30% voltage drop (t : 0.5 s/div).

The waveforms with existing and proposed VSC are given in Figure 7a,b, respectively. As shown in Figure 7, when the voltage of the power grid drops by 30%, the PW current also drops firstly and then raises sharply. At the voltage-drop moment, the transient PW flux is introduced, so the PW current oscillates and finally damps to the new stable value. At the voltage drop moment, the CW current is also impacted by the PW flux. In the proposed control, as Figure 7b shows, the compensation current term can restrain the oscillation better than that of the existing control. It is noted that in both cases, the active power of the BDFIG system injected into the grid is reduced. Therefore, the mechanical power and active power are unbalanced and the rotor speed is increased. Besides, the grid-side current of the B2B converter is limited at 1.2 pu, so the grid-side converter cannot maintain a stable voltage of dc-link in the B2B converter. The extra short-term energy storage units are thus active to control the dc-link voltage. Nevertheless, the emergency rotor control will be activated to reduce the mechanical power and finally achieve power balancing of the whole BDFIG system again.

As shown in Figure 8, when the voltage of the power grid drops, the BDFIG can also inject about 0.46 pu reactive power into the grid to support grid recovery. It is worth mentioning that at the transient process of voltage drop, the active power changes its direction. This is because the compensation term in the proposed control aims to restrain the oscillation of the CW current, rather than that of the PW current, and thus, cannot ensure the direction of active power during the transient process. This phenomenon can also be found in [25]; nevertheless, it can be regulated again after the transient process, which can be observed in Figure 8.

The waveforms with a 70% voltage drop are given in Figure 9, and conclusions similar to those in Figure 7 can still be obtained. Especially, the deep voltage drop results in larger PW- and CW-current oscillations with the existing control; while with the proposed control, these oscillations can still be well-restrained. It should be mentioned that with a deep voltage drop, the unbalancing of mechanical power, active power, and dc-link voltage will be worse. Thanks to the extra short-term energy storage units and the emergency rotor control, the whole BDFIG system can work stably. As shown in Figure 10, the BDFIG with proposed control can still inject reactive power into the grid to support the voltage recovery, but the amount of reactive power becomes 0.25 pu, which simulates the behavior of SG well.

Deviations of compensation terms might introduce uncertainties during control. Therefore, two situations where the current compensation exhibits -20% and $+20\%$ deviations are also considered, as shown in Figure 11. It is seen that such deviations will slightly impact the restraining effect, but the control system is still stable.

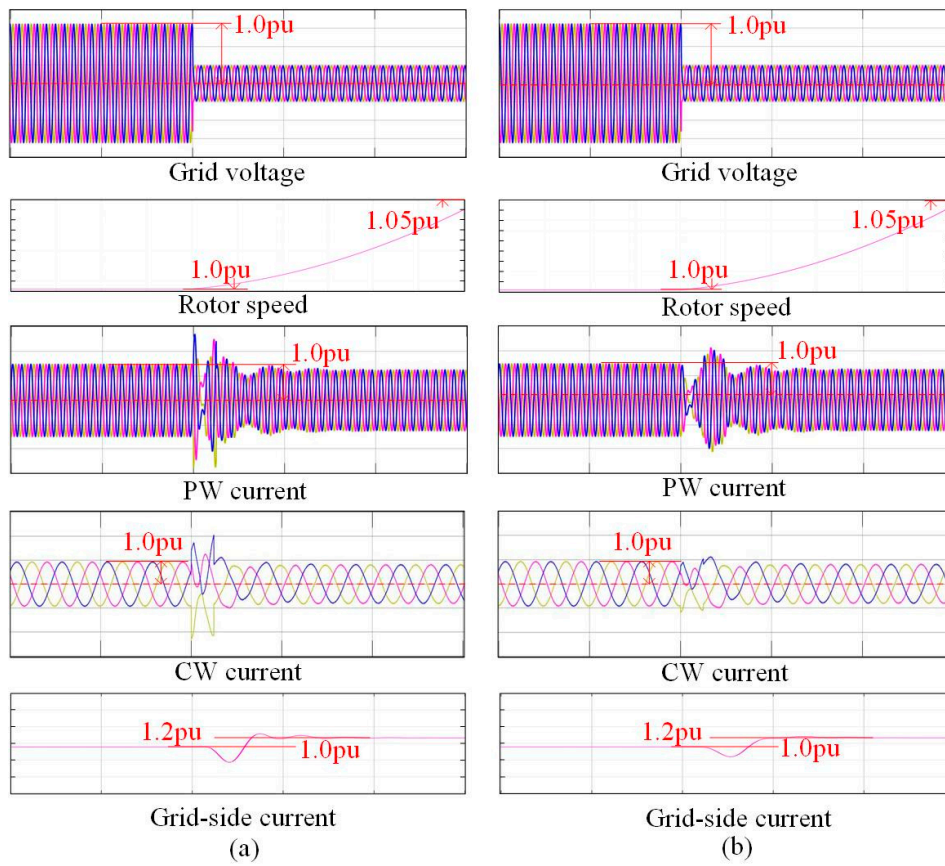


Figure 9. Comparison of waveforms when the grid has a 70% voltage drop with (a) existing VSC and (b) the proposed VSC ($t: 0.2 \text{ s/div}$).

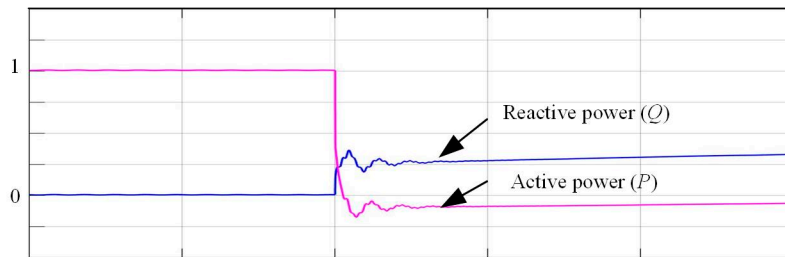


Figure 10. Waveforms of active and reactive power with 70% voltage drop ($t: 0.5 \text{ s/div}$).

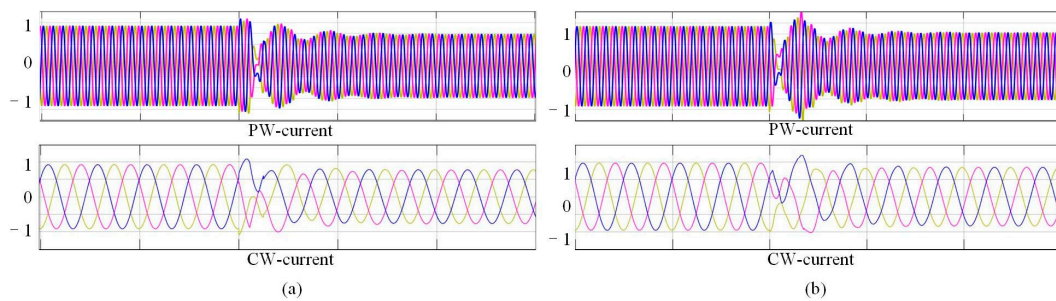


Figure 11. The PW and CW waveforms when the compensation is (a) -0.2 and (b) $+0.2$ deviations.

6. Conclusions

This paper studies the VSC of BDFIG and introduces a CW transient current compensation based on CW current oriented vector control. The proposed control strategy makes the BDFIG simulate the behavior of SG. The following merits have been proved:

1. The proposed VSC control can be easily realized by adding the VSC block and current compensation block into the original CW current oriented vector control system. The control strategy does not need to be switched when the grid fault occurs;
2. The over CW current introduced by a symmetrical grid fault has been well-restrained, which maintains the safety operation of the BDFIG system; the control can inject a certain reactive power into the grid during a grid fault, which supports the grid voltage recovery;
3. With the extra short-term energy storage units and emergency rotor control, the proposed VSC has a good inertial support ability since it simulates the behavior of SG.

The proposed control only utilizes the reactive capacity of the BDFIG to support grid voltage recovery; however, the reactive power can also be provided by the grid-side of the B2B converter. This issue is not considered in this study. Besides, the method in [26] could be referred so that the active power during the voltage drop can maintain its direction.

Author Contributions: M.L. designed the principles of the overall work, realized MATLAB-based simulation, and prepared the initial draft of the paper. Y.C. proposed the basic idea and significantly contributed to writing the paper. D.Z. and J.S. edited the initial draft of the paper. Y.K. proposed some technical comments and edited the final draft of the paper.

Funding: This research was funded by the Natural Science Foundation of China, grant number 51467018 and The Power Electronics Science and Education Development Program of Delta Environmental & Educational Foundation, grant number DREM2015001.

Conflicts of Interest: The authors declare no conflict of interest.

References

1. Negnevitsky, M.; Potter, C.W. Innovative short-term wind generation prediction techniques. In Proceedings of the Power Conference and Exposition, Atlanta, GA, USA, 29 October–1 November 2006; pp. 60–65.
2. Valentine, S.V. A STEP toward understanding wind power development policy barriers in advanced economies. *Renew. Sustain. Energy Rev.* **2010**, *14*, 2796–2807. [[CrossRef](#)]
3. Lee, C.K.; Bhang, B.G.; Kim, D.K.; Lee, S.H.; Cha, H.L.; Ahn, H.K. Estimation of Load Pattern for Optimal Planning of Stand-alone Microgrid Networks. *Energies* **2018**, *11*, 2012. [[CrossRef](#)]
4. Abolude, A.T.; Zhou, W. Assessment and Performance Evaluation of a Wind Turbine Power Output. *Energies* **2018**, *11*, 1992. [[CrossRef](#)]
5. Shao, S.; Abdi, E.; Barati, F.; McMahan, R. Stator-Flux-Oriented Vector Control for Brushless Doubly Fed Induction Generator. *IEEE Trans. Ind. Electron.* **2009**, *56*, 4220–4228. [[CrossRef](#)]
6. Barati, F.; Shao, S.; Abdi, E.; Oraee, H.; McMahan, R. Generalized Vector Model for the Brushless Doubly-Fed Machine with a Nested-Loop Rotor. *IEEE Trans. Ind. Electron.* **2011**, *58*, 2313–2321. [[CrossRef](#)]
7. Zhongshan, J.; Sai, W.; Xiaopeng, R. Simulation Study of Vector Control Strategy for Stand-alone BDFG System. *Micromotors* **2014**, *47*, 48–51.
8. Poza, J.; Oyarbise, E.; Roye, D.; Rpdriquez, M. Unified reference frame dq model of the brushless doubly fed machine. *IEE Proc. Electr. Power Appl.* **2006**, *153*, 726–734. [[CrossRef](#)]
9. Long, T.; Shao, S.; Malliband, P.; Abdi, E.; McMahan, R.A. Crowbarless Fault Ride-Through of the Brushless Doubly Fed Induction Generator in a Wind Turbine Under Symmetrical Voltage Dips. *IEEE Trans. Ind. Electron.* **2013**, *60*, 2833–2841. [[CrossRef](#)]
10. Shipurkar, U.; Strous, T.D.; Polinder, H.; Ferreira, J.A. LVRT performance of brushless doubly fed induction machines A comparison. In Proceedings of the 2015 IEEE International Electric Machines & Drives Conference (IEMDC), Coeur d’Alene, ID, USA, 10–13 May 2015; pp. 362–368.

11. Liu, C.; Yu, C.; Wang, Q.; Zhang, W. The LVRT control ability analysis of BDFIG motor side converter. In Proceedings of the 2017 32nd Youth Academic Annual Conference of Chinese Association of Automation (YAC), Hefei, China, 19–21 May 2017; pp. 1239–1243.
12. Nie, P.; Wang, X.; Wu, W. Research on low voltage ride through of brushless doubly-fed wind power generator. In Proceedings of the 2016 19th International Conference on Electrical Machines and Systems (ICEMS), Chiba, Japan, 13–16 November 2016; pp. 1–6.
13. Kerdphol, T.; Rahman, F.S.; Mitani, Y. Virtual Inertia Control Application to Enhance Frequency Stability of Interconnected Power Systems with High Renewable Energy Penetration. *Energies* **2018**, *11*, 981. [[CrossRef](#)]
14. Beltran, O.; Pena, R.; Segundo, J.; Esparza, A.; Muljadi, E.; Wenzhong, D. Inertia Estimation of Wind Power Plants Based on the Swing Equation and Phasor Measurement Units. *Appl. Sci.* **2018**, *8*, 2413. [[CrossRef](#)]
15. Yu, Z.; Ai, Q.; He, X.; Piao, L. Adaptive Droop Control for Microgrids Based on the Synergistic Control of Multi-Agent Systems. *Energies* **2016**, *9*, 1057. [[CrossRef](#)]
16. Ghefiri, K.; Bouallegue, S.; Garrido, I.; Garrido, A.J.; Haggege, J. Complementary Power Control for Doubly Fed Induction Generator-Based Tidal Stream Turbine Generation Plants. *Energies* **2017**, *10*, 862. [[CrossRef](#)]
17. Zheng, Z.; Yang, G.; Geng, H. Coordinated Control of a Doubly-Fed Induction Generator-Based Wind Farm and a Static Synchronous Compensator for Low Voltage Ride-through Grid Code Compliance during Asymmetrical Grid Faults. *Energies* **2013**, *6*, 4660–4681. [[CrossRef](#)]
18. Wu, H.; Ruan, X.; Yang, D.; Chen, X.; Zhao, W.; Lv, Z.; Zhong, Q. Small-Signal Modeling and Parameters Design for Virtual Synchronous Generators. *IEEE Trans. Ind. Electron.* **2016**, *63*, 4292–4302. [[CrossRef](#)]
19. Visscher, K.; DeHaan, S.W.H. Virtual synchronous machines (VSG's) for frequency stabilization in future grids with a significant share of decentralized generation. In Proceedings of the CIRED Seminar 2008: SmartGrids for Distribution, Frankfurt, Germany, 23–24 June 2008; pp. 1–4.
20. Ma, Y.; Cao, W.; Yang, L.; Wang, F.; Tolbert, L.M. Virtual Synchronous Generator Control of Full Converter Wind Turbines with Short-Term Energy Storage. *IEEE Trans. Ind. Electron.* **2017**, *64*, 8821–8831. [[CrossRef](#)]
21. Wang, S.; Hu, J.; Yuan, X. On Inertial Dynamics of Virtual-Synchronous-Controlled DFIG-Based Wind Turbines. *IEEE Trans. Energy Convers.* **2015**, *30*, 1691–1702. [[CrossRef](#)]
22. Tangyun, M. *Electrical Motor*; China Machine Press: Beijing, China, 2014.
23. Lu, M.; Chen, Y.; Sun, L.; Zou, X.D.; Kang, Y. Control Winding Quantities Orientation Modeling and Control for Stand-alone Brushless Doubly-Fed Power Generation System. In Proceedings of the 2015 IEEE Energy Conversion Congress and Exposition, Montreal, CANADA, Montreal, QC, Canada, 20–24 September 2015.
24. Cheng, X.; Sun, X.; Chai, J.; Zhao, Y. Virtual Synchronous Control Strategy for Doubly-fed Induction Generator Under Asymmetrical Grid Faults. *Autom. Electr. Power Syst.* **2018**, *42*, 120–126.
25. Hang, C.; Wang, X.; Liu, N. Virtual Inductance Control Strategy for Brushless Doubly-fed Induction Generator During Grid Voltage Dips. In Proceedings of the 2018 21st International Conference on Electrical Machines and Systems (ICEMS), Jeju, Korea, 7–10 October 2018.
26. Shang, L.; Hu, J.; Yuan, X.; Chi, Y.; Tang, H. Modeling and Improved Control of Virtual Synchronous Generators Under Symmetrical Faults of Grid. *Proc. CSEE* **2017**, *32*, 403–411.

